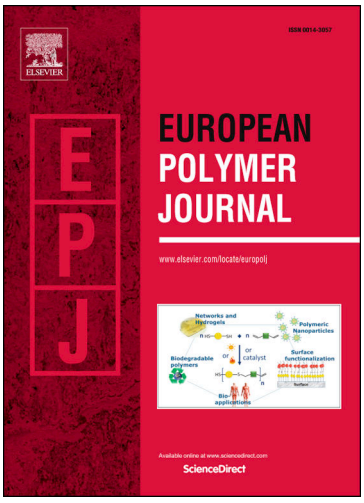

Advancing sustainable shape memory polymers through 4D printing of polylactic acid-polybutylene adipate terephthalate blends

Davood Rahmatabadi, Mahdi Khajepour, Abbas Bayati, Kiandokht Mirasadi, Mohammad Amin Yousefi, Atefeh Shegeft, Ismaeil Ghasemi, Majid Baniassadi, Karen Abrinia, Mahdi Bodaghi, Mostafa Baghani

PII: S0014-3057(24)00550-0
DOI: https://doi.org/10.1016/j.eurpolymj.2024.113289
Reference: EPJ 113289

To appear in: *European Polymer Journal*

Received Date: 17 May 2024
Revised Date: 30 June 2024
Accepted Date: 8 July 2024

Please cite this article as: Rahmatabadi, D., Khajepour, M., Bayati, A., Mirasadi, K., Amin Yousefi, M., Shegeft, A., Ghasemi, I., Baniassadi, M., Abrinia, K., Bodaghi, M., Baghani, M., Advancing sustainable shape memory polymers through 4D printing of polylactic acid-polybutylene adipate terephthalate blends, *European Polymer Journal* (2024), doi: https://doi.org/10.1016/j.eurpolymj.2024.113289

Advancing Sustainable Shape Memory Polymers through 4D Printing of Polylactic Acid-Polybutylene Adipate Terephthalate Blends

Davood Rahmatabadi[1], Mahdi Khajepour[1], Abbas Bayati[1], Kiandokht Mirasadi[1], Mohammad Amin Yousefi[1], Atefeh Shegeft[2], Ismaeil Ghasemi[2], Majid Baniassadi[1], Karen Abrinia[1], Mahdi Bodaghi[3*], and Mostafa Baghani[1*]

[1] School of Mechanical Engineering, College of Engineering, University of Tehran, Tehran, Iran

[2] Faculty of Processing, Iran Polymer and Petrochemical Institute, Tehran, Iran

[3] Department of Engineering, School of Science and Technology, Nottingham Trent University, Nottingham NG11 8NS, UK

[*]Corresponding authors: mahdi.bodaghi@ntu.ac.uk; baghani@ut.ac.ir

- 3D/4D printing of novel biodegradable PLA-PBAT blends
- Direct printing by Granule-based FDM printer with low cost
- Achieving fast shape recovery in less than a few seconds (4 s)
- Excellent softening of PLA with PBAT resulting in over 200% elongation
- Achieving excellent thermo-mechanical properties and shape memory effects

Abstract

One of the major challenges in 4D printed Shape Memory Polymers (SMPs) is their slow response to thermal stimuli. Synthetic carbon fillers have been introduced to address this issue; however, their use comes with environmental concerns. On the other hand, Polylactic Acid (PLA) is commonly used for 3D/4D printing of SMPs, but it requires softening to achieve large deformations. This research paper introduces a sustainable solution through blending PLA with Polybutylene Adipate Terephthalate (PBAT) that not only addresses these challenges but also possesses environmental eco-friendliness due to PBAT's high biodegradability rate. PBAT with weight percentages of 15%, 30%, and 45% is utilized to soften PLA, and their composites are successfully 4D printed. Mechanical properties, shape memory effects, morphology, and thermal behaviors are comprehensively investigated. The results show that blending PLA with 45% PBAT weight results in excellent features such as 220% elongation and 93% shape recovery in just a few seconds. The other two PLA-PBAT blends achieve complete shape recovery in less than 8 seconds. The PLA-PBAT contains 15% PBAT, in addition to high strength (40 MPa), has 17% elongation. This, coupled with the low melting temperature of PBAT, drives the high shape recovery rate. Scanning electron microscopy images finally confirm the high printability of all three blends, with the PLA-PBAT composite containing 30% PBAT exhibiting the best quality in layer interfaces and the least porosity.

Keywords: 3D/4D Printing; Shape Memory Polymers; Polylactic Acid; Polybutylene Adipate Terephthalate; Shape Recovery

1. Introduction

Three-dimensional (3D) printing, also known as additive manufacturing (AM), is a digital manufacturing process that involves adding materials layer by layer to create 3D objects directly from computer-aided design (CAD) models [1]. 3D printing technology was first introduced in the late 1980s. Since then, it has become increasingly popular due to its capacity to manufacture complex components efficiently by reducing material waste and production time [2]. This innovative technology has found applications in diverse fields such as biomedical sciences and aerospace. A variety of AM methods are available for 3D printing using a wide range of materials, including metals, polymers, composites, and ceramics [3]. One of the most popular 3D printing methods for creating polymer parts is Fused Deposition Modeling (FDM). FDM involves layering thermoplastic polymer on a build platform to create parts in a precise and efficient manner.

While 3D printing offers many advantages over traditional manufacturing methods, one significant limitation is that printed parts are typically static. The gap between static printed parts and dynamic printed parts was bridged by the invention of four-dimensional (4D) printing [4]. This innovative technology adds a new dimension (time) to printed structures by utilizing shape memory materials (SMMs), a type of smart material used in 3D printing [5]. Shape Memory Polymers (SMPs), as the most common Smart materials, can react to external stimuli such as heat [6,7], electric fields [8], magnetic fields [9,10], light [11], and more. 4D printed structures can change their physical and chemical properties, such as stiffness and density, and can demonstrate Shape Memory Effect (SME) [12]. This effect is a phenomenon in which a system or structure can remember a specific shape and transition from one shape to another (initial shape to programmed shape) in a controlled manner in the presence of external stimuli [13]. Among SMPs, thermal stimulation is generally used more than others. Thermoresponsive SMPs are a category of smart polymeric materials capable of reverting from a deformed state to their permanent shape when subjected to a change in temperature [14]. The typical mechanism of thermoresponsive SMPs involves four steps: (1) The deformation of the SMP at a specific temperature known as the glass transition temperature (T_g) of the switching units, (2) Keeping the load constant, lowering the temperature below T_g, (3) Releasing the load to restore the temporary shape, and (4) Reheating the material to its T_g to restore its original shape from the deformed state. This four-step sequence, leading to the restoration of shape, constitutes a thermomechanical cycle [15].

Along with Acrylonitrile butadiene styrene (ABS), Polylactic acid (PLA) is the most widely used commercial thermoplastic for 3D printing for routine applications such as rapid prototyping. What distinguishes PLA from ABS is its biocompatibility, biodegradability, and shape memory properties. PLA is a biodegradable SMP that responds to changes in temperature. It has become widely popular in 4D printing due to its versatility in 3D printing and its cost-effectiveness [16,17]. In 4D printing, PLA is the most widely used commercial shape memory thermoplastic. PLA has a transition temperature of approximately 60-70°C [18]. The crystalline domains and molecular entanglements act as net points and determine its original permanent shape. What makes PLA superior to amorphous SMPs is the stronger net points due to its semi-crystalline structure. This makes it show a higher stress relaxation resistance and is more suitable for commercial applications. But the excessive brittleness of PLA makes it impossible to apply high deformation at application temperatures, especially lower than its transition temperature. For this reason, the use of PLA-based blends for practical applications is more common than pure PLA. PLA-TPU, PLA-PCL [19,20], PLA-SEBS [21], PLA-PEG [22], PLA-NR [23], PLA-PBS [24,25] and PLA-

PBAT [26] are among the most common PLA blends in the field of 3D printing and recently 4D printing. Ádám et al. [21] conducted a study on the effects of adding 1-5% SEBS (styrene ethylene-butylene styrene) thermoplastic elastomer to PLA. They investigated the thermal and mechanical properties of the resulting blends. The study revealed that incorporating a small amount of SEBS improved the impact strength without reducing the tensile modulus. Fekete et al. [23] investigated the suitability of PLA-based blends toughened with natural rubber (NR) for FDM additive manufacturing applications. The results of their research showed that the presence of NR significantly effectively increased the ductility of PLA filaments. However, the improvement obtained was highly dependent on the filler pattern applied. Rahmatabadi et al. [27] blended TPU with PLA through melt mixing and then FDM 3D-printing method in different percentages of content. The research findings showed that flexibility increased while strength decreased with higher TPU content in all loading modes. Additionally, the study found a decrease in fracture toughness with an increase in TPU content. In another study [28], they investigated SME by examining how the loading mode and temperature influence on the three PLA-TPU compounds: 50-50%, 70-30%, and 90-10% by weight. The findings of their study revealed as the concentration of PLA increased, the level of shape recovery also increased, (reaching 96.4% for the sample with 70% PLA concentration). Additionally, the cold-programmed samples exhibited the highest and lowest shape fixity and recovery ratios. Of course, the sample with the lowest amount of TPU could not be cold programmed.

By blending PLA with biodegradable and eco-friendly plastics like Polybutylene Adipate Terephthalate (PBAT), the resulted blend becomes a sustainable solution for a wide range of applications due to the enhanced mechanical properties compared to pure PLA. This is because PBAT enhances the flexibility and increases the toughness of PLA [29]. In addition to its excellent softening effect, PBAT has a high biodegradability rate [30], and unlike most of the mentioned PLA blends, PLA-PBAT can be superior to pure PLA in terms of biodegradability and sustainability. Kumar et al. [31] utilized the melt blending technique to prepare the PLA-PBAT blend. Their findings revealed a notable increase in both impact strength and tensile properties of the PLA matrix with higher PBAT loading. Furthermore, the incorporation of glycidyl methacrylate (GMA) was observed to significantly enhance the impact strength of the blend. Bianchi et al. [32] investigated the microstructural, thermomechanical, and shape memory properties of biodegradable PLA-PBAT blends. They produced these blends by melt mixing at varying relative amounts. The findings revealed that the stiffness and strength of the blends decrease as the PBAT concentration increases. In contrast, higher PBAT concentrations led to a significant increase in the ductility of the mixture, with elongation at break reaching up to 83.8% at a PBAT content of 75 wt%. Furthermore, the study recorded a shape fixity ability of 77.3% and a recovery ability of 73.6% with a PBAT content of 30% by weight. Andrzejewski et al. [33] investigated the potential use of PLA-PBAT compounds in FDM printing. Their study demonstrated the enhanced properties of PLA-PBAT compared to pure PLA. The optimum tensile strength, impact toughness, and rheological properties were achieved in the PLA-PBAT composite containing 30% PBAT and through reactive extrusion using a 0.5phr chain extender. Cardoso et al. [34] conducted a study to analyze how various FDM printing parameters impact the porosity and flexural properties of components made from PLA-PBAT blends. They employed an experimental design approach to determine the optimal parameter set for achieving the best results. The findings indicated that utilizing lower printing parameter values led to the production of parts with reduced porosity and improved bending properties. Chen et al. [35] investigated the degradation effects of PLA-PBAT polymer blends, emphasizing their significance for

biodegradable materials. Blends were prepared via solution casting, and subsequent analyses revealed that while Young's modulus remained reasonably stable, the tensile strain was significantly reduced with ongoing degradation, signifying a decline in mechanical performance. Additionally, thermal stability was adversely impacted. SEM images showed micrometer-scale defects, enhancing understanding of PLA-PBAT degradation for future material improvements.

Furthermore, PBAT presents a distinct advantage over conventional plasticizers utilized in 3D printed PLA; its notably low melting temperature. This characteristic significantly accelerates the thermal stimulation required for efficient 4D printing processes. Unlike conventional approaches reliant on synthetic carbon-based fillers to enhance thermal responsiveness in SMPs, our current study pioneers the utilization of PBAT. In this research, PBAT was strategically incorporated into PLA at three varying weight percentages (15%, 30%, and 45%), enabling the attainment of several groundbreaking objectives: (a) tailoring PLA softness and mechanical properties to cater to diverse applications, (b) augmenting the biodegradability rate of PLA, and (c) expediting the shape recovery kinetics within 4D printed structures. This innovative approach not only enhances the performance of PLA-based SMPs but also underscores a sustainable pathway towards advanced additive manufacturing methodologies, especially 4D printing.

2. Materials and Methods

2.1. Materials

The raw materials used in this study for preparing PLA-PBAT blends were PLA granules of 2003D grade from the Nature works with a molecular weight of 42,700 g/mol, as well as PBAT granules of KD 1024 grade a molecular weight of 52,100 g/mol from the Zhuhai Wango Chemical Co. The raw materials were then subjected to a dehumidification process in an oven at 60°C and 40°C for 9 hours.

2.2. Preparation of PLA-PBAT Blends

Three types of PLA-PBAT blends were processed in this investigation, with PBAT constituting 15%, 30%, and 45% by weight in each blend. The raw materials were fused and homogenized using a Brabender internal mixer with a capacity of 60 cc. The process involved pouring PLA granules into the mixer at 170 °C for two minutes until fully melted, followed by the addition of PBAT granules. The blends were then left in the device for 10 minutes to ensure a uniform structure, with the speed set at 60 rpm. The resulting materials were lumpy polymer blends. Sheets were formed from the mixed materials using a hot press machine at a temperature of 170°C for 5 minutes, and then for an additional 10 minutes under a pressure of 60 kPa in a cold press machine. Finally, the produced sheets were converted into granules in preparation for 3D printing.

2.3. 3D Printing

The PLA-PBAT blends were 3D-printed using the FDM method with a new-generation printer. Unlike traditional printers that require filament extraction for printing, this printer functions by directly introducing raw material granules into the thermal chamber through a pneumatic system. By utilizing direct granule printing and eliminating the filamentation process, the material undergoes one fewer thermomechanical procedure, leading to potential enhancements in its mechanical, thermal, and SME. This improvement can be attributed to the significant influence of

thermal and stress history on the properties of polymers. With this printing method, the granules are melted inside the cartridge and attain suitable rheology in a semi-melted form before being guided into the nozzle using air pressure for printing. The printing temperature of the PLA-PBAT was selected based on the printing temperature of PLA, and then due to the reduction of melting temperature with the addition of PBAT, the printing temperature was reduced to provide optimal printing conditions. The basic parameters of FDM printing for these blends are detailed in Table 1.

Table 1. Optimized Parameters for 3D Printing PLA-PBAT Blends

Printing Parameters	Values
Velocity (mm/min)	300
Nozzle Temperature (℃)	180±15
Bed Temperature (℃)	25
Nozzle Diameter (mm)	0.6
Layer Thickness (mm)	0.45
Printing Direction	0-90
Air pressure (Bar)	2-4

2.4. DMTA

The 3D-printed samples underwent Dynamic Mechanical Thermal Analysis (DMTA) using a Mettler Toledo dynamic thermomechanical device from Switzerland. The analysis was conducted following the ASTM D4065-01 standard for a three-point bending load, at a frequency of 1 Hz. The temperature range spanned from -100 °C to 100 °C, with a heating rate of 1 °C/min. The samples were rectangular, measuring 40*10 mm in length.

2.5. Mechanical Properties

The mechanical properties of all three PLA-PBAT blends were comprehensively assessed using the ASTM D638 type V standards for tensile loading. All tests were conducted at ambient temperature with a displacement rate of 1 mm/min and were repeated at least three times to ensure repeatability.

2.6. Morphology and Printability

Imaging was performed using a scanning electron microscope to analyze the bond quality between the PLA-PBAT layers. Before imaging, the samples were fragmented using liquid nitrogen and then coated with gold. The imaging process was conducted using the Vegall model SEM manufactured by Tescan Company.

2.7. Shape memory behavior of 3D printed PLA/PBAT blend

The PLA-PBAT blends underwent an evaluation for their SME in bending loading mode, which included programming and recovery stages. The programming process involved heating, loading, cooling, and unloading the printed samples. The shape fixity(R_f), can be calculated using the Equation 1:

$$R_f = \frac{\varepsilon_{Fixed}}{\varepsilon_{Applied}} \times 100$$

To restore the original shape, the deformed samples were reheated to a temperature above the T_g. Once the sample temperature enters to the transition and then rubber region, the shape recovery process begins. The shape recovery parameter is determined using the Equation 2:

$$R_r = \frac{\varepsilon_{Recoverd}}{\varepsilon_{Fixed}} \times 100$$

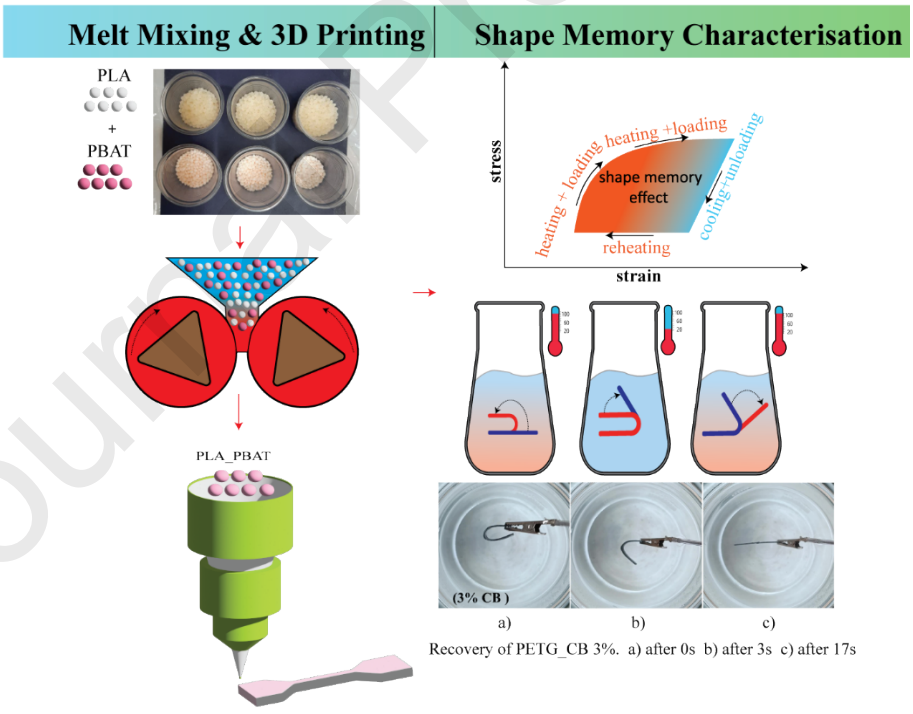

Figure 1. Different stages of preparation, 3D and 4D printing of PLA-PBT blends

The test parts were beam-shaped with dimensions of 50*10 mm and a thickness of 1.5 mm. The samples were heated in water at 80 °C for 120 seconds, and then subjected to bending loading.

Subsequently, the samples were stabilized in water at 20 °C and the load was removed. Water at a temperature of 80 °C was used in the recovery process. To ensure accuracy, shape recovery tests were repeated three times for all samples. In Figure 1, the different stages of preparation by melt mixing method, 3D printing and evaluation the shape memory effect are presented.

3. Results and Discussion

3.1. DMTA

Figure 2 illustrates the variations of Tan δ for the PLA-PBAT blends across temperatures from -100 °C to 100 °C. Tan δ represents the relationship between the loss modulus (reflecting viscous properties) and the storage modulus (reflecting elastic properties) [36]. This metric, as defined in Equation 3, helps evaluate the material's ability to absorb and release energy under external forces, which is crucial for understanding the material's shape memory behavior.

$$Tan\delta = \frac{E''}{E'}$$

If Tan δ is greater than 1, it indicates that the material exhibits more viscous behavior than elastic behavior. Conversely, if Tan δ is less than 1, the material's elastic behavior is dominant. A higher Tan δ value suggests that the material is better at absorbing and dissipating energy rather than storing and recovering it [37]. Figure 2 illustrates that as the proportion of PBAT in the blend increases, the elastic behavior becomes more dominant. This shift is attributed to the molecular structures of the blend components depicted in Figure 3.

PLA is composed of repetitive lactic acid units, featuring a relatively rigid structure with methyl groups on one side and a hydroxyl group on the other. These characteristics result in strong intermolecular forces between the polymer chains, promoting a dense and ordered molecular arrangement [38]. These robust intermolecular forces restrict the mobility of polymer chains, impeding their ability to slide past one another. Consequently, PLA demonstrates significant stiffness and rigidity. In contrast, PBAT is characterized by flexible aliphatic chain and aromatic groups in its composition. The presence of flexible aliphatic segments within PBAT allows for enhanced freedom of movement between polymer chains, leading to a less tightly packed and more flexible molecular structure compared to PLA [39]. The parameter Tan δ provides insights into transitions occurring in polymers. Peaks observed in Tan δ correspond to polymer chain movements and transitions [40]. These transitions, particularly the glass-rubber transition, are integral to the material's shape memory behavior because the temperature at which these transitions take place serves as the switching temperature for shape recovery.

Below the glass transition temperature (Tg), polymer chains are constrained in a relatively rigid state with restricted mobility. With higher temperatures and increased free volume in the polymer structure, polymer chains gain enhanced mobility and flexibility. This allows them to move, rotate, and slide more easily past each other, transitioning from an orderly and rigid state to a disordered and rubbery state as they approach the glass-transition temperature [41].

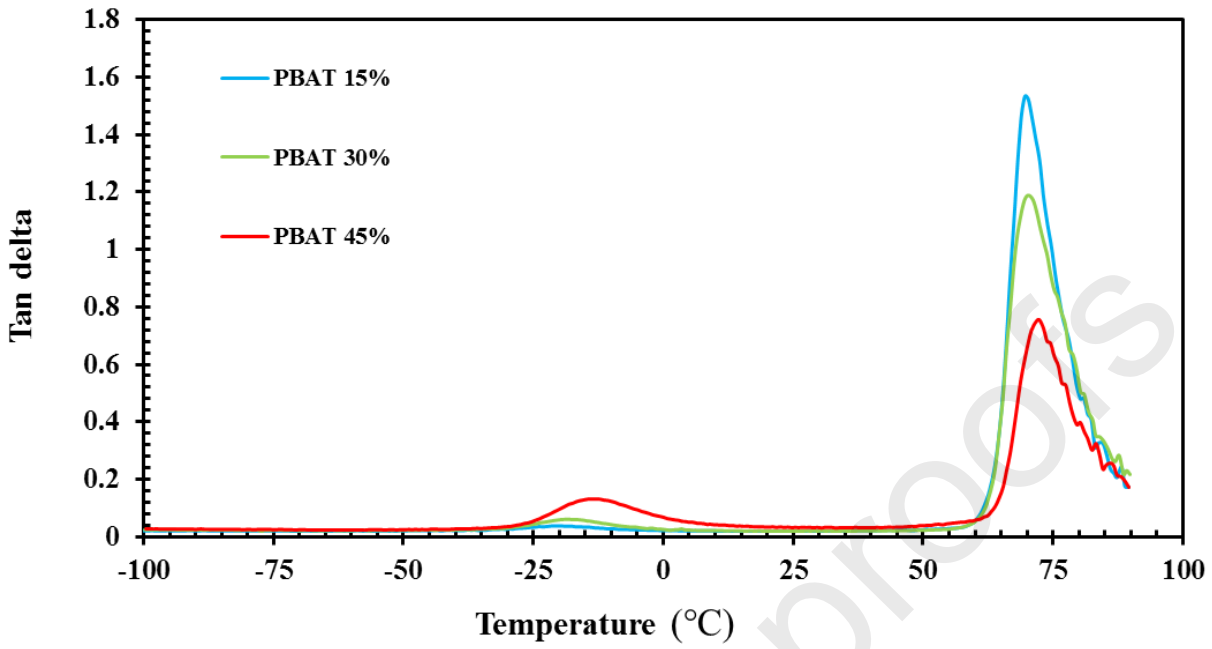

Figure 2. Tan δ of PLA-PBAT blends

The glass transition temperature (Tg) of PLA is higher than that of PBAT due to the ordered and rigid nature of PLA chains and the flexible nature of PBAT chains. In PLA-PBAT blends, two peaks of Tan δ can be detected in -15 °C and 75 °C. These peaks correspond to the respective glass transition temperatures of the individual components (PBAT and PLA) within the blend.

The first peak, which is related to the glass transition temperature of the PBAT, is more intense for the sample containing more PBAT, and this trend can also be seen for the second peak. Therefore, in the range of the first and second transition temperatures, the PLA-PBAT blends containing 45% and 15% by weight of PBAT, respectively, have higher peak intensity. These two peaks indicate the immiscibility and biphasic nature of all three PLA-PBAT blends, and the changes in the peaks and the approach of the transition temperatures of each phase compared to the pure state indicate the acceptable compatibility of the two phases. Prior studies support these findings [26].

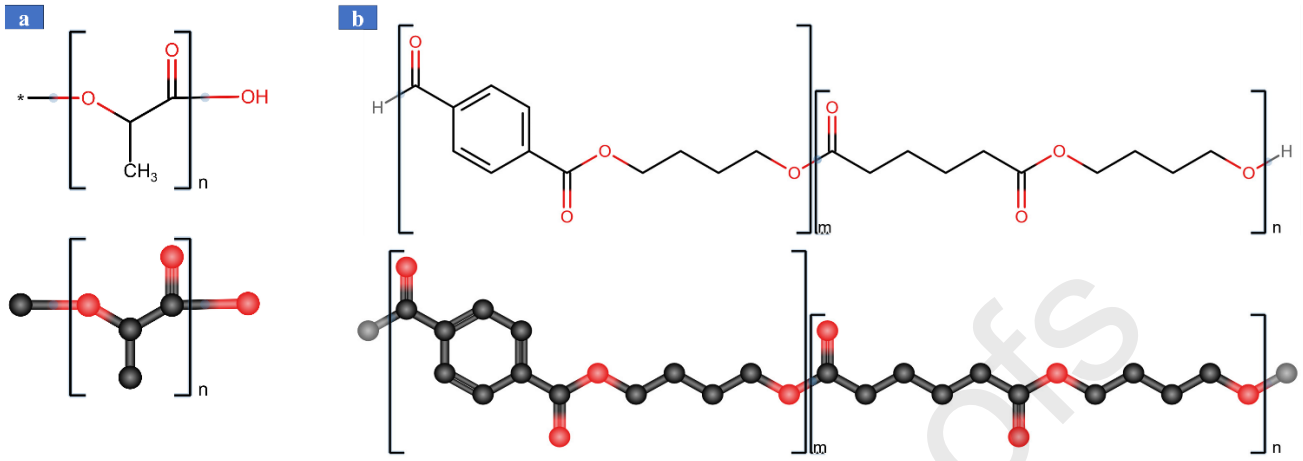

Figure 3. Molecular structure of (a) PLA and (b) PBAT

Figure 4(a) displays the change in storage modulus across a temperature range from -100 °C to 100 °C. In addition, these changes in the log scale are presented in Figure 4(b). Below the glass transition temperature (Tg), the material exhibits a glassy state where the storage modulus is high due to limited chain mobility [42]. All blends exhibit a storage modulus of approximately 2000-2500 MPa in this region which is less than neat PLA. Upon reaching Tg, the storage modulus decreases as the material's chain mobility increases, rendering it more flexible. This decline occurs twice in the blends, indicating two distinct Tg points and phases. The initial decrease in storage modulus is associated with the Tg of PBAT, ranging from -25 °C to 0 °C. In this region, the peak in neat PLA is not observed and it confirms that this peak is due to the addition of PBAT. Blend with 45% PBAT exhibit the most pronounced decrease in modulus, followed by blend with 30% PBAT, whereas blend with 15% PBAT display a minor decrease. This observation suggests that the phase transition in PBAT occurs in this temperature, and blends with higher PBAT content are more significantly influenced by this transition. At room temperature, blends containing higher proportions of PLA demonstrate a more rigid behavior (higher storage modulus). When the temperature reaches 60 °C, the second transition begins, and it is completed at approximately 75 °C. This transition is caused by the change in chain mobility in the PLA phase. Consequently, blends with a higher PLA content are more affected by this transition, leading to a more significant drop in storage modulus in these blends. A noticeable drop in modulus for neat PLA is also observed in this area.

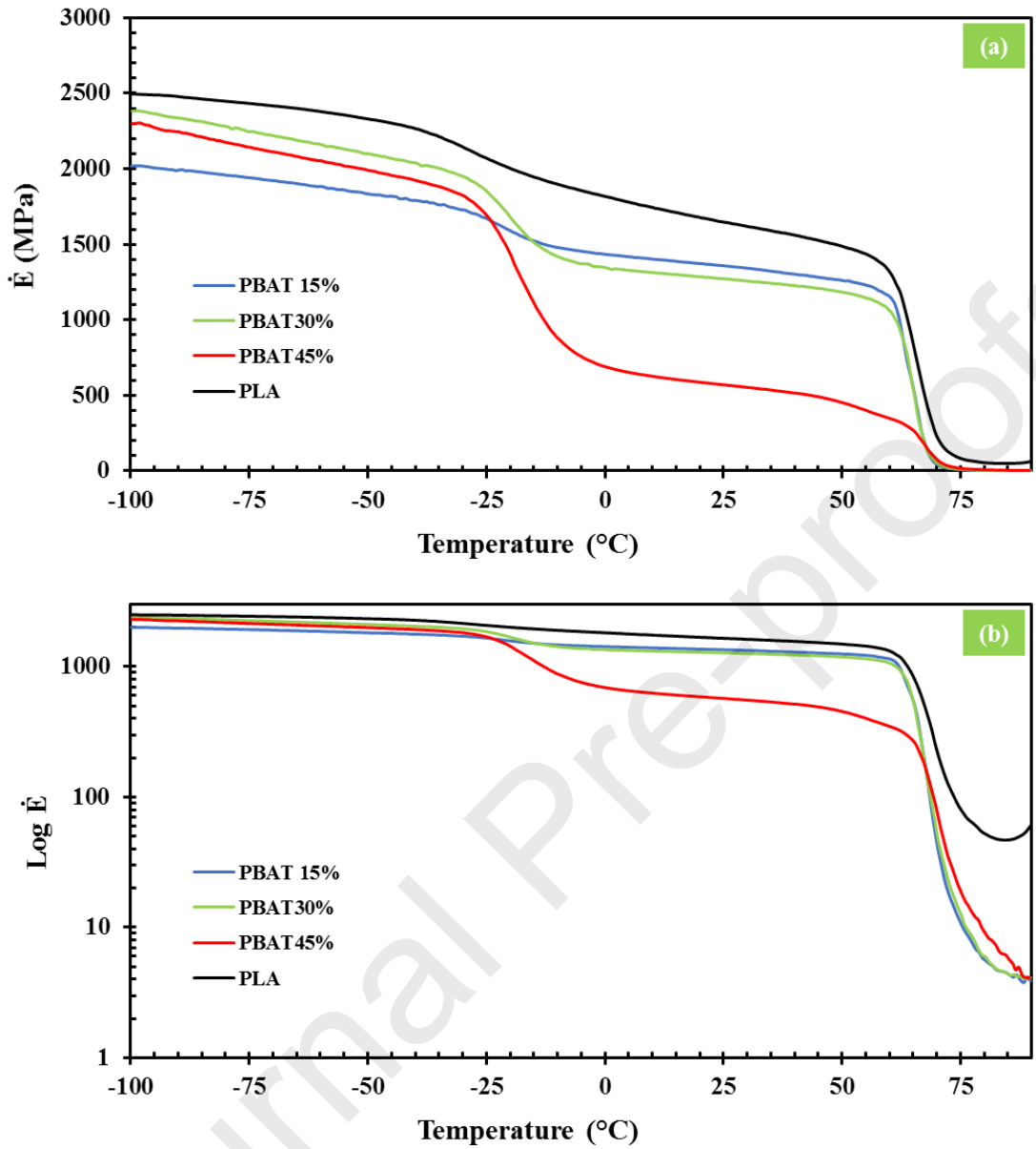

Figure 4. storage modulus of PLA-PBAT blends: (a) linear and (b) log scales

3.2. Printability

Due to the layer-by-layer fabrication process of molten polymer in 3D printing, it is essential to maintain a high level of adhesion between the layers to improve the mechanical properties of the final 3D printed products [43]. The adhesion between layers of FDM components is facilitated by the heat energy present in the partially melted material [44]. In addition to this, printing parameters can also strongly affect the quality of bonding layers and the formation of microholes. Of course, it has been tried to remove this effect by printing the PLA-PBAT blends with the same and optimal printing parameters.

The SEM analysis of the PLA-PBAT blends reveals distinct morphological characteristics that are indicative of the printability of the materials. The images captured at magnifications of 35x, 50x, and 100x provide a comprehensive view of the liquid nitrogen fractured surfaces of the tensile specimens, allowing for a detailed comparison of the blends with varying percentages of PBAT (15%, 30%, and 45%).

In the first set of images Figure 5 (a-c), representing PLA-PBAT-15%, the micrographs exhibit a relatively higher number of voids among layers, which are distributed throughout the matrix. These voids serve as favorable locations for crack nucleation and possess the potential to considerably impact the mechanical properties of the printed specimens [2]. Conversely, the second set of Figure 5 (d-f) corresponding to PLA-PBAT-30% indicates a marked reduction in the number of voids. This observation is particularly evident in the 50x magnification, where the voids appear to be smaller and less frequent. The rise in PBAT content in the PLA-PBAT blend is thought to boost the coefficient of volume expansion of the blend, making it easier for the melted layers to adhere during 3D printing and continue to build layer by layer. The third set of Figure 5 (g-i) for PLA-PBAT-45% demonstrates a further decrease in void size, yet an increase in their number, especially noticeable at 100x magnification. This could be attributed to the higher PBAT content, which may promote a finer dispersion within the PLA matrix but also introduce more voids due to phase separation.

Consequently, comparing the three sets of blends, it becomes apparent that PLA-PBAT-30% is the most optimal concentration for printability, as it offers the best combination of material homogeneity and mechanical properties, making it the most suitable candidate for high-quality, printable applications. This finding is instrumental for guiding the development of PLA-PBAT blends with enhanced printability for advanced manufacturing processes.

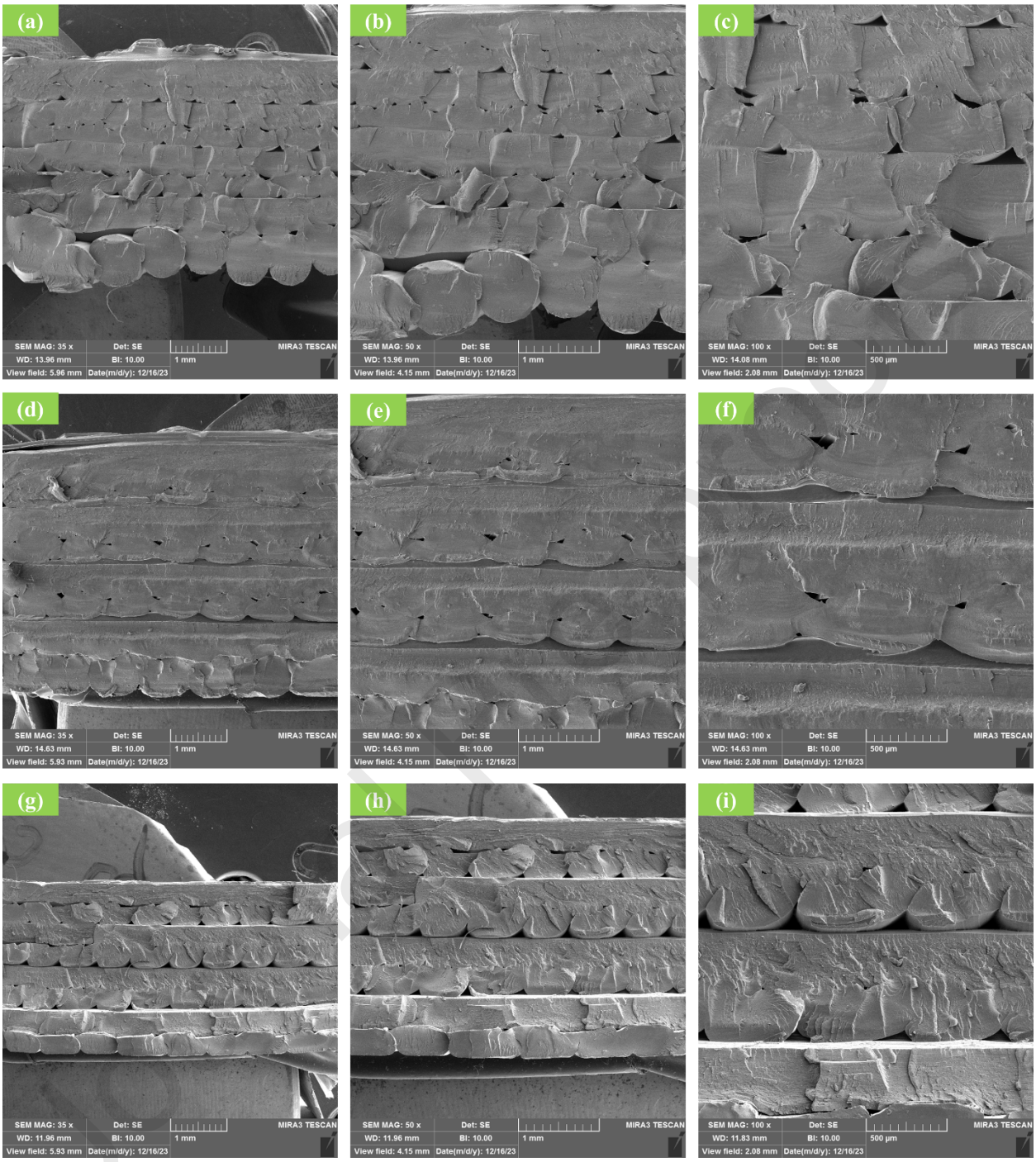

Figure 5. SEM printability analysis of PLA-PBAT blends (85/15 (a-c), 70/30 (d-f), 55/45 (g-i)) at various magnifications (35x, 50x, 100x)

3.3. Morphology

SEM micrographs of the gold coated fracture surface of the PLA-PBAT blends with 15% and 45% PBAT content are displayed in Figure 6. A typical "sea-island" morphology is observed in both sets of images, with the PBAT phase dispersed as spherical domains within the PLA matrix. This phase separation indicates immiscibility between the PLA and PBAT polymers, agreeing with previous studies in the literature and DMTA results [26,45,46].

At 5000x magnification, the PLA-PBAT-15% blend (Figure 6(a)) exhibits a lower density of PBAT spheres compared to the PLA-PBAT-45% blend (Figure 6(c)). The size distribution of the dispersed PBAT phase also appears more uniform in the 15% sample. As the PBAT content is increased to 45%, the spherical domains become larger and more non-uniformly distributed. At a magnification of 10000x, some coalescence of neighboring PBAT spheres can also be observed, leading to the formation of particles with diameters ranging from 2 to 5 μm for the PLA-PBAT-45 blend. It is noteworthy to mention that in the PLA-PBAT-15% blend, these particles are notably smaller, measuring less than 0.5 μm in diameter.

The density and size distribution of the dispersed PBAT phase provide insight into the blend miscibility and viscoelastic properties. The lower density but more uniform PBAT spheres in the PLA-PBAT-15% blend indicate a finer dispersion with greater interfacial area between the phases. In contrast, the higher PBAT content of the 45% blend promotes sphere coalescence and non-uniform distributions. The maintained spherical geometry of PBAT across both compositions suggests a lack of interfacial adhesion with the PLA matrix. In terms of properties, the finer dispersed morphology of lower PBAT contents would promote opacity, gas permeability, and fatigue resistance of the PLA-PBAT blends [47]. The larger domains and coalescence at higher 45% PBAT loadings can act as stress concentrators, reducing mechanical integrity. However, they may enhance ductility due to the initiation of shear yielding. These regions of the PBAT with different geometries and weak junctions are marked with a green outline in Figure 6(d).

Therefore, the SEM analysis demonstrates that PBAT wt% significantly influences the sea-island morphology in PLA-PBAT blends. Based on the viscosity ratio calculation, a co-continuous phase structure was anticipated to emerge at a PBAT concentration of 19 wt%, leading to a significant improvement in ductility [48]. This prediction is supported by our observation that lower PBAT loadings of 15% generate finer dispersions with more uniform sphere size distributions compared to 45% PBAT. The morphological variations with composition impact opacity, gas barrier, mechanical and viscoelastic performance. However, interfacial adhesion remains low even at high PBAT contents, as evidenced by the maintained spherical particle shapes.

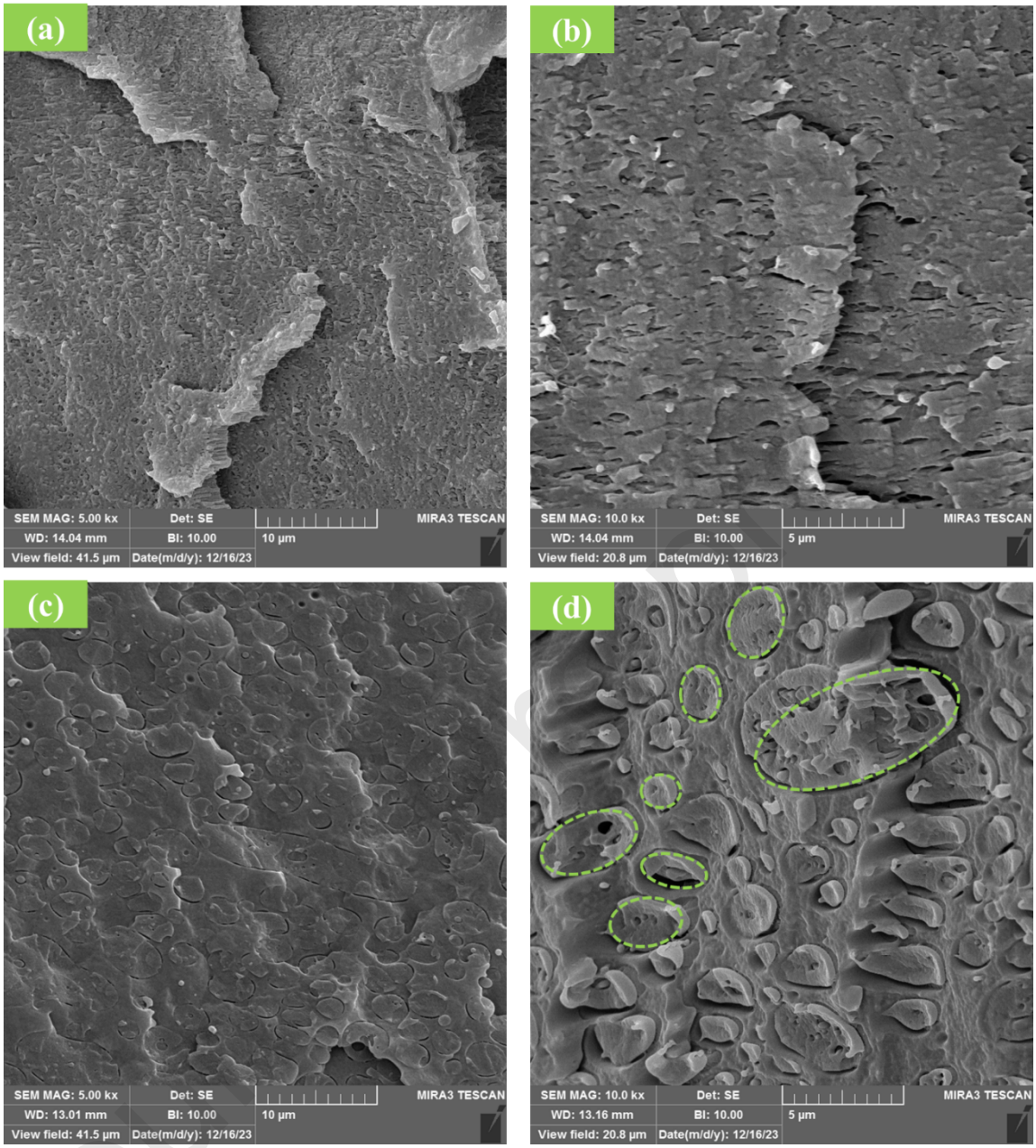

Figure 6. SEM morphology analysis of PLA-PBAT blends (85/15 (a-b), 55/45 (c-d)) at various magnifications (5000 x, 10000 x)

3.4. Mechanical Properties

Figure 7 presents the tensile test diagrams for PLA-PBAT blends produced via 3D printing. The stress-strain diagrams indicate that as the PBAT amount increases, the slope of the linear region (Young's modulus) and tensile strength decreases but elongation increases. Remarkably, the PLA-PBAT15% blend exhibits superior tensile strength while the PLA-PBAT45% blend shows the maximum elongation. In other words, the softening role of PBAT on PLA can be seen well. In this regard, increasing the percentage of PBAT decreases Young's modulus and ultimate tensile strength (UTS) simultaneously. In immiscible or biphasic blends, the role of the phase with lower

strength (weaker phase) is very effective in failure. In these blends, usually the beginning of different stages of failure starts from the weaker phase or the interfaces of two phases. During loading, the PBAT phase undergoes deformation and with the increase of strain, microcracks are created and spread in the interface or weaker points. The failure of the sample is occurred by connecting the cracks and expanding them. With the increase of the PBAT volume in PLA-PBAT blends, the elastic part that supports more deformation increases. On the other hand, the blends containing more PLA shows a stiffer behavior and yields at a higher stress level. Specifically, according to Figure 8 (a), the tensile strength values for 3D printed PLA-PBAT blends containing 15%, 30%, and 45% by weight of PABT are 39.96 MPa, 30.93 MPa, and 29.29 MPa, respectively.

Figure 8 (b) shows the changes in uniform and total elongation (strain values at UTS and fracture point) for 3D printed PLA-PBAT blends in terms of weight percentage of PBAT. Based on this examination, it is evident that all three blends exhibit nearly identical uniform elongation; while a significant distinction arises in terms of total elongation. PLA-PBAT blends containing 15%, 30%, and 45% PBAT demonstrate total elongation of 16.84%, 36.65%, and 227.49%, and the uniform elongation for these blends are about 7.14%, 7.42% and 8.12% respectively. This result proved that the softening effect of PBAT shows itself after the UTS point and causes a significant increase in plasticity. The change in uniform elongation can be the beginning of microcracks in the PBAT phase, which is almost the same in all samples. But the total elongation is due to the stretching of the PBAT phase in the direction of applying tension and bringing the microcracks together until the final failure.

The toughness behavior (absorbed energy or area under the stress-strain diagram during a tensile test) of the 3D printed PLA-PBAT blends, up to UTS and fracture points, is depicted in Figure 8 (c). Similar to the mechanical properties, it can be seen that up to UTS strain, all blends behave similarly. However, the main difference between these three blends appears in the amount of fracture strain. According to extracted quantitative results, for the PLA-PBAT blends with the percentage of PBAT 45%, 30%, and 15%, the values of total toughness are approximately equal to 45kJ, 10kJ, and 5kJ respectively.

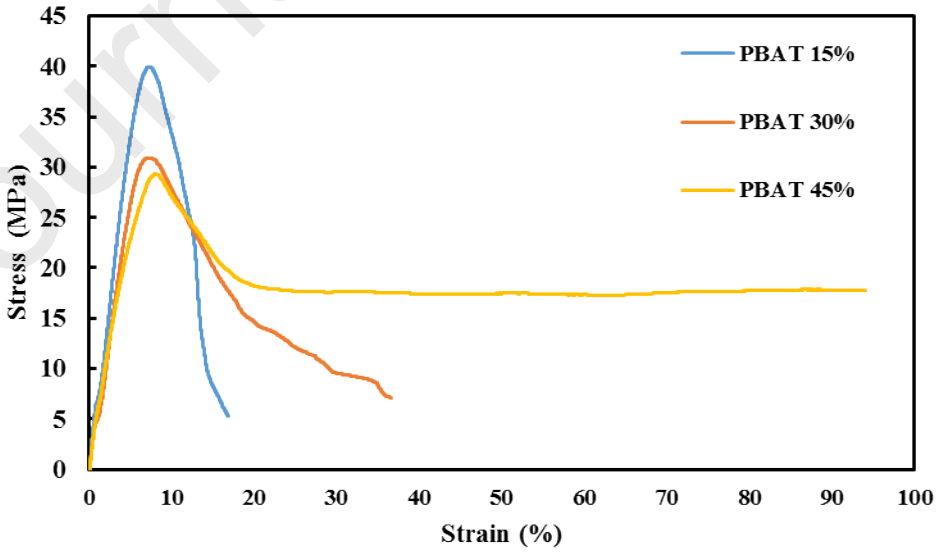

Figure 7. Stress-strain curves of 3D printed PLA-PBAT blends

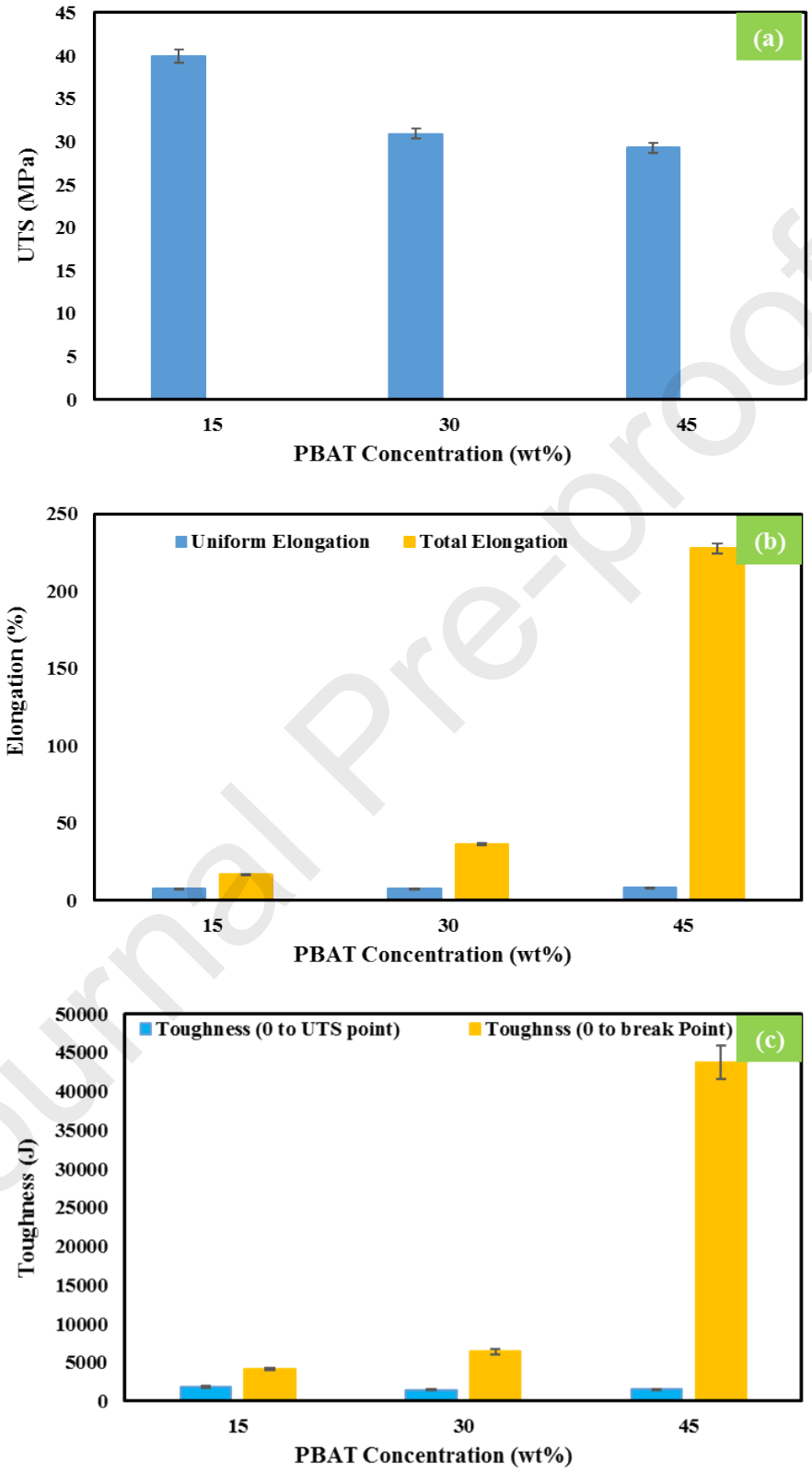

Figure 8. Quantitative data extracted from tensile test: (a) tensile strength, (b) elongation and (c) toughness

3.5. Shape Memory Effect

The analysis of the shape memory effect, including the shape fixity and shape recovery visually was performed for the additively manufactured PLA-PBAT blends in boiling water. The shape recovery was imaged according to Figure 9 and then quantitative data was extracted including shape recovery ratio according to time. The remarkable feature is the shape recovery of all three PLA-PBAT blends samples in a very short time and quick response to heat and according to the Figures, the shape recovery is done in less than 8 seconds.

Notably, Figure 10 showcases the shape recovery results under thermal stimulation, revealing a substantial disparity in both the quantity and duration of shape recovery among the blends. Considering Figure 10, a clear trend emerges with the increase of PBAT leading to a significant reduction in recovery time. The PLA-PBAT45% blend sample achieves over 90% shape recovery in less than 2 seconds. Similarly, the PLA-PBAT30% attains a shape recovery value exceeding 90% after 4 seconds, while the PLA-PBAT15% sample reaches the same threshold after 5 seconds. These results are also compared with pure PLA and this comparison suggest a substantial decrease in recovery time with adding an increased percentage of PBAT, indicating that a PLA-PBAT45% recovers 250% faster than PLA-PBAT15% to surpass the 90% recovery ratio. In addition to reducing the transition temperature and reducing the elastic modulus, the increase in PBAT increases the recovery rate due to the reduction of hard points and molecular entanglements in the PLA segments. In other words, by reducing the volume of PLA with a higher transition temperature and more hard points in PLA-PBAT blends, the energy required for shape recovery is reduced and at a lower temperature, the level of energy required for recovery is provided. For this reason, the increase in PBAT is associated with a decrease in shape recovery time (increase in recovery rate). This trend of shape recovery changes has already been observed in PLA blends samples [28].

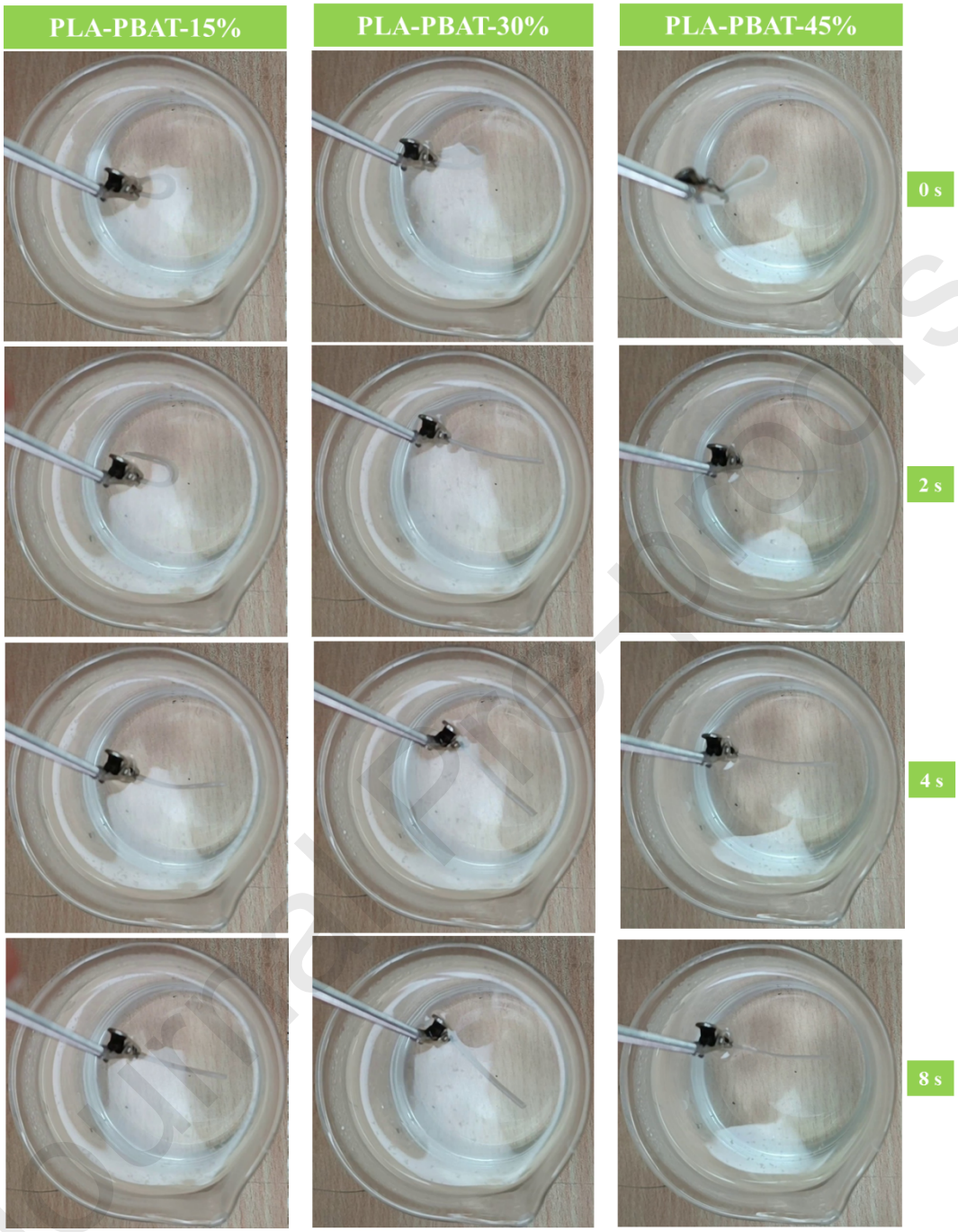

Figure 9. Frames of shape recovery in terms of time for PLA-PBAT blends

Moreover, the results indicate that after 8 seconds, lower percentages of PBAT correlate with higher shape recovery ratios. This implies that while increasing PBAT enhances recovery speed, it concurrently leads to a lower shape recovery ratio. As mentioned, the elastic modulus decreases with the increase of PBAT, and with the increase of recovery temperature, this decreasing process becomes more intense. Therefore, with the passage of time and the temperature of the blends becoming uniform to higher than the melting temperature of the PBAT segments (above 70 °C), the shape recovery is done only by the hard part of PLA, and with the increase of PLA, a higher

percentage of recovery is obtained. Of course, according to the recovery frames and quantitative results, the shape recovery values of each PLA-PBAT blends are acceptable (above 90%) and significant.

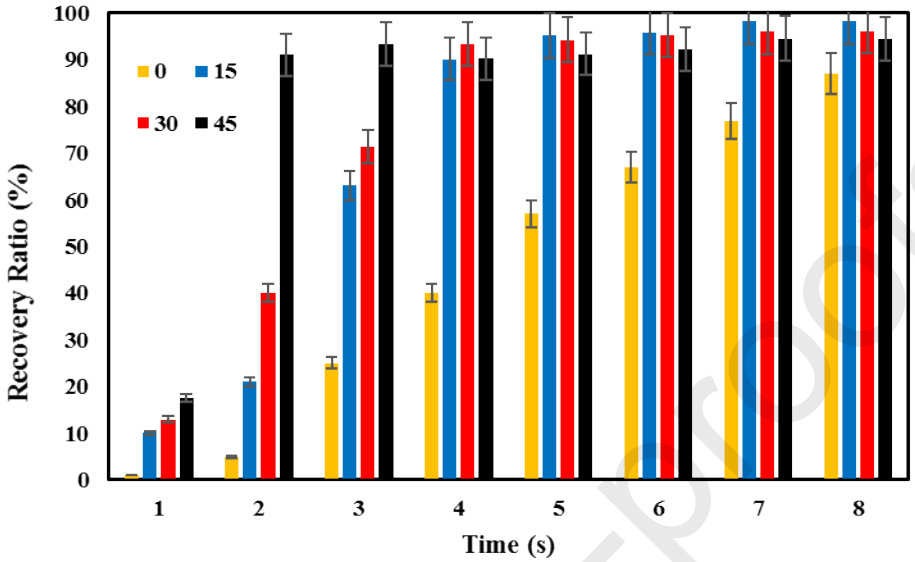

Figure 10. Quantitative data extracted from the shape memory test. Shape recovery in terms of time for neat PLA and PLA-PBAT blends

The SME observed in PLA-PBAT blends can be explained using the DMTA storage modulus diagram, as depicted in Figure 11. In the shape memory process of PLA-PBAT blends, the glass transition temperature (Tg) of PLA serves as the switching temperature. Initially, the printed PLA/PBAT blends are cooled to room temperature, then heated above the Tg of PLA, causing all blends to become rubbery and flexible. At this stage, the blends are programmed into a temporary shape and subsequently cooled to retain this programmed shape. The difference in storage modulus between the rubbery and glassy states is critical for shape fixity, with higher fixity observed in blends with a higher PLA content due to a greater modulus difference [49–51].

Following this, the samples are reheated above the Tg to recover their permanent shape. Blends with a lower PBAT content, such as PLA-PBAT15%, are expected to recover faster due to a smaller difference in storage modulus between the rubbery and glassy states, albeit with lower shape recovery. Conversely, blends with a higher PLA content exhibit slower recovery but demonstrate superior shape recovery, attributed to the substantial difference in moduli between the glassy and rubbery states.

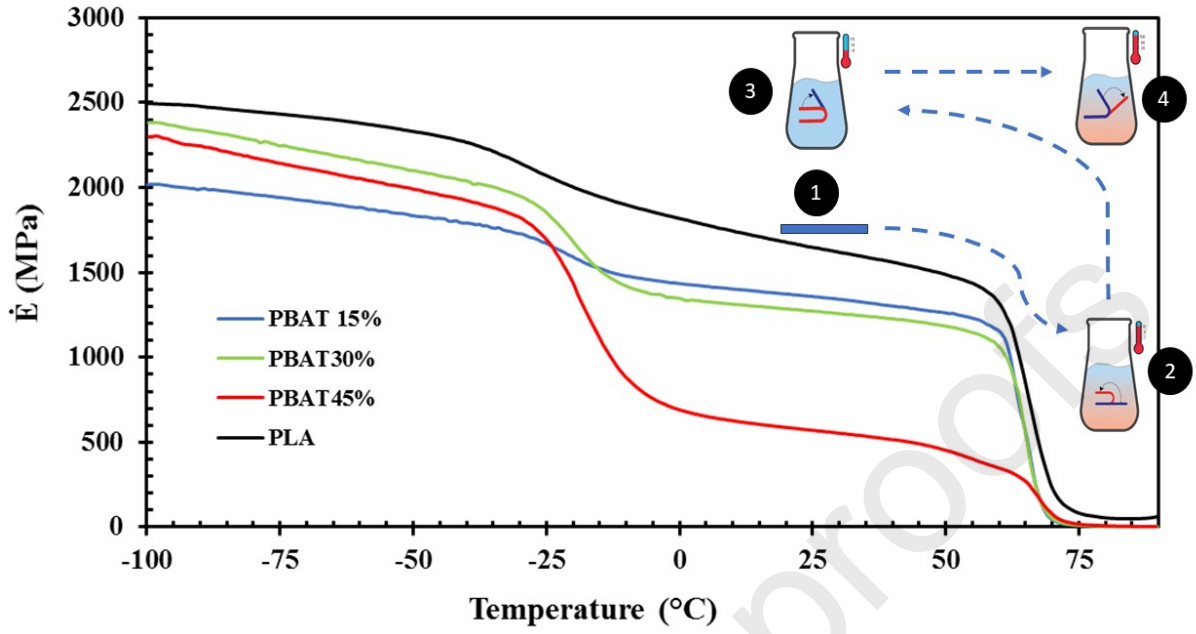

Figure 11. Shape memory effect observed in neat PLA and PLA-PBAT blends explained using the DMTA storage modulus diagrams

4- Conclusion

This paper aimed to enhance the thermo-mechanical properties of PLA for sustainable 4D printing applications by incorporating PBAT, characterized by its high biodegradability and low melting temperature. Three PLA-PBAT blends (15%, 30%, and 45% by weight of PBAT) were prepared using the melt mixing method and successfully 3D/4D printed using the FDM technique. The study encompassed comprehensive analysis including DMTA, mechanical properties, shape memory performance under thermal stimulation, and evaluation of layer bonding, interface quality, and morphology using SEM. The key findings and highlights of this study are summarized as follows:

- The SEM and DMTA results confirm that the PLA-PBAT blends are two-phase and immiscible, and with the increase in the amount of PBAT, the compatibility between the two phases decreases, and this factor can be the reason for the decrease in the printability of the blend containing 45% PBAT by weight.
- SEM images showed that all 3D printed blends have good printing quality, which can be due to the ability to control the output flow with the new pneumatic system on the FDM printer. Also, the sample containing 30% PBAT by weight had the least micro-holes between the grids and the quality of the layers' connection was excellent.
- The results of mechanical properties revealed an increase in tensile strength with the increase of PLA, although the amount of uniform and final elongation showed an almost neutral and completely opposite trend with the increase of PLA. PLA-PBAT blends containing 15%, 30%, and 45% PBAT demonstrated total elongation of 16.84%, 36.65%, and 227.49%, and the uniform elongation for these blends were about 7.14%, 7.42% and 8.12% respectively

- The difference in the tensile strength levels and the high difference in the total elongation values, respectively, caused the amount of energy absorbed in the UTS and fracture points to have the same process as the change in tensile strength and total elongation for PLA-PBAT blends.
- By increasing the amount of PBAT, the time of the shape recovery decreases drastically, and for the PLA-PBAT blends with 45% by weight of PBAT, and the shape recovery of more than 90% was observed in less than a few seconds. In addition, the increase of PBAT caused a slight decrease in the shape recovery rate, although all three blends had shape recovery values above 90%.

Data Availability:

The data will be made available upon request from the corresponding authors.

Acknowledgment:

Mahdi Bodaghi acknowledges the supported by the Engineering and Physical Sciences Research Council (EPSRC) [Grant No. EP/Y011457/1].

References

[1] Karimi A, Rahmatabadi D, Baghani M. Various FDM Mechanisms Used in the Fabrication of Continuous-Fiber Reinforced Composites: A Review. Polymers (Basel) 2024;16:831. https://doi.org/10.3390/polym16060831.

[2] Bayati A, Rahmatabadi D, Ghasemi I, Khodaei M, Baniassadi M, Abrinia K, et al. 3D printing super stretchable propylene-based elastomer. Mater Lett 2024;361:136075. https://doi.org/10.1016/J.MATLET.2024.136075.

[3] Dezaki ML, Bodaghi M. 4D printing and programming of continuous fibre-reinforced shape memory polymer composites. Eur Polym J 2024;210:112988. https://doi.org/10.1016/j.eurpolymj.2024.112988.

[4] Shinde S, Mane R, Vardikar A, Dhumal A, Rajput A. 4D printing: From emergence to innovation over 3D printing. Eur Polym J 2023;197:112356. https://doi.org/10.1016/J.EURPOLYMJ.2023.112356.

[5] Akbar I, El Hadrouz M, El Mansori M, Lagoudas D. Toward enabling manufacturing paradigm of 4D printing of shape memory materials: Open literature review. Eur Polym J 2022;168:111106. https://doi.org/10.1016/J.EURPOLYMJ.2022.111106.

[6] Jeong HY, Lee E, Ha S, Kim N, Jun YC. Multistable Thermal Actuators Via Multimaterial 4D Printing. Adv Mater Technol 2019;4:1–7. https://doi.org/10.1002/admt.201800495.

[7] Rahmatabadi D, Soltanmohammadi K, Pahlavani M, Aberoumand M, Soleyman E, Ghasemi I, et al. Shape memory performance assessment of FDM 3D printed PLA-TPU composites by Box-Behnken response surface methodology. Int J Adv Manuf Technol 2023;127:935–50. https://doi.org/10.1007/s00170-023-11571-2.

[8] Zeng C, Liu L, Bian W, Liu Y, Leng J. 4D printed electro-induced continuous carbon fiber reinforced shape memory polymer composites with excellent bending resistance. Compos Part B Eng 2020;194:108034. https://doi.org/10.1016/J.COMPOSITESB.2020.108034.

[9] Zhao W, Zhang F, Leng J, Liu Y. Personalized 4D printing of bioinspired tracheal scaffold concept based on magnetic stimulated shape memory composites. Compos Sci Technol 2019;184:107866. https://doi.org/10.1016/j.compscitech.2019.107866.

[10] Lalegani Dezaki M, Bodaghi M. Sustainable 4D printing of magneto-electroactive shape memory polymer composites. Int J Adv Manuf Technol 2023:1–14. https://doi.org/10.1007/S00170-023-11101-0/FIGURES/8.

[11] Jeong HY, Woo BH, Kim N, Jun YC. Multicolor 4D printing of shape-memory polymers for light-induced selective heating and remote actuation. Sci Rep 2020;10:1–11. https://doi.org/10.1038/s41598-020-63020-9.

[12] Bodaghi M, Serjouei A, Zolfagharian A, Fotouhi M, Rahman H, Durand D. Reversible energy absorbing meta-sandwiches by FDM 4D printing. Int J Mech Sci 2020;173:105451. https://doi.org/10.1016/j.ijmecsci.2020.105451.

[13] Soleyman E, Aberoumand M, Rahmatabadi D, Soltanmohammadi K, Ghasemi I, Baniassadi M, et al. Assessment of controllable shape transformation, potential applications, and tensile shape memory properties of 3D printed PETG. J Mater Res Technol 2022;18:4201–15. https://doi.org/10.1016/J.JMRT.2022.04.076.

[14] Li H, Gao Y, Zhao S, Gao W, He X, Cong R, et al. Dual and triple shape memory properties of poly(ε-caprolactone)-based cross-linked polymer elastomers. Polym Test 2022;115:107738. https://doi.org/10.1016/J.POLYMERTESTING.2022.107738.

[15] Li G, Xu W. Thermomechanical behavior of thermoset shape memory polymer programmed by cold-compression: Testing and constitutive modeling. J Mech Phys Solids 2011;59:1231–50. https://doi.org/10.1016/J.JMPS.2011.03.001.

[16] Bhagia S, Bornani K, Agarwal R, Satlewal A, Ďurkovič J, Lagaňa R, et al. Critical review of FDM 3D printing of PLA biocomposites filled with biomass resources, characterization, biodegradability, upcycling and opportunities for biorefineries. Appl Mater Today 2021;24:101078. https://doi.org/10.1016/J.APMT.2021.101078.

[17] Sun L, Wang TX, Chen HM, Salvekar AV, Naveen BS, Xu Q, et al. A Brief Review of the Shape Memory Phenomena in Polymers and Their Typical Sensor Applications. Polym 2019, Vol 11, Page 1049 2019;11:1049. https://doi.org/10.3390/POLYM11061049.

[18] Rahmatabadi D, Soltanmohammadi K, Aberoumand M, Soleyman E, Ghasemi I, Baniassadi M, et al. 4D printing of porous PLA-TPU structures: effect of applied deformation, loading mode and infill pattern on the shape memory performance. Phys Scr 2024;99:025013. https://doi.org/10.1088/1402-4896/AD1957.

[19] Yao B, Zhu Y, Xu Z, Wu Y, Yang L, Liu J, et al. Taguchi design and optimization of the PLA/PCL composite filament with plasticizer and compatibilizer additives for optimal 3D printing. Polym Eng Sci 2023;63:3743–61. https://doi.org/10.1002/PEN.26481.

[20] Åkerlund E, Diez-Escudero A, Grzeszczak A, Persson C. The Effect of PCL Addition on 3D-Printable PLA/HA Composite Filaments for the Treatment of Bone Defects. Polymers (Basel) 2022;14:3305. https://doi.org/10.3390/POLYM14163305/S1.

[21] Ádám B, Weltsch Z. Thermal and Mechanical Assessment of PLA-SEBS and PLA-SEBS-CNT Biopolymer Blends for 3D Printing. Appl Sci 2021, Vol 11, Page 6218 2021;11:6218. https://doi.org/10.3390/APP11136218.

[22] Kumar R, Alex Y, Nayak B, Mohanty S. Effect of poly (ethylene glycol) on 3D printed PLA/PEG blend: A study of physical, mechanical characterization and printability assessment. J Mech Behav Biomed Mater 2023;141:105813. https://doi.org/10.1016/J.JMBBM.2023.105813.

[23] Fekete I, Ronkay F, Lendvai L. Highly toughened blends of poly(lactic acid) (PLA) and natural rubber (NR) for FDM-based 3D printing applications: The effect of composition and infill pattern. Polym Test 2021;99:107205. https://doi.org/10.1016/J.POLYMERTESTING.2021.107205.

[24] Ou-Yang Q, Guo B, Xu J. Preparation and Characterization of Poly(butylene succinate)/Polylactide Blends for Fused Deposition Modeling 3D Printing. ACS Omega 2018;3:14309–17. https://doi.org/10.1021/ACSOMEGA.8B02549/ASSET/IMAGES/MEDIUM/AO-2018-02549J_0008.GIF.

[25] Yu W, Sun L, Li M, Li M, Lei W, Wei C. FDM 3D Printing and Properties of PBS/PLA Blends. Polym 2023, Vol 15, Page 4305 2023;15:4305. https://doi.org/10.3390/POLYM15214305.

[26] Lyu Y, Chen Y, Lin Z, Zhang J, Shi X. Manipulating phase structure of biodegradable PLA/PBAT system: Effects on dynamic rheological responses and 3D printing. Compos Sci Technol 2020;200:108399. https://doi.org/10.1016/J.COMPSCITECH.2020.108399.

[27] Rahmatabadi D, Ghasemi I, Baniassadi M, Abrinia K, Baghani M. 3D printing of PLA-TPU with different component ratios: Fracture toughness, mechanical properties, and morphology. J Mater Res Technol 2022;21:3970–81. https://doi.org/10.1016/j.jmrt.2022.11.024.

[28] Rahmatabadi D, Ghasemi I, Baniassadi M, Abrinia K, Baghani M. 4D printing of PLA-TPU blends: effect of PLA concentration, loading mode, and programming temperature on the shape memory effect. J Mater Sci 2023 2023:1–17. https://doi.org/10.1007/S10853-023-08460-0.

[29] Wang X, Peng S, Chen H, Yu X, Zhao X. Mechanical properties, rheological behaviors, and phase morphologies of high-toughness PLA/PBAT blends by in-situ reactive compatibilization. Compos Part B Eng 2019;173:107028. https://doi.org/10.1016/J.COMPOSITESB.2019.107028.

[30] Singamneni S, Behera MP, Truong D, Le Guen MJ, Macrae E, Pickering K. Direct extrusion 3D printing for a softer PLA-based bio-polymer composite in pellet form. J Mater Res Technol 2021;15:936–49. https://doi.org/10.1016/J.JMRT.2021.08.044.

[31] Kumar M, Mohanty S, Nayak SK, Rahail Parvaiz M. Effect of glycidyl methacrylate (GMA) on the thermal, mechanical and morphological property of biodegradable PLA/PBAT blend and its nanocomposites. Bioresour Technol 2010;101:8406–15.

https://doi.org/10.1016/J.BIORTECH.2010.05.075.

[32] Bianchi M, Dorigato A, Morreale M, Pegoretti A. Evaluation of the Physical and Shape Memory Properties of Fully Biodegradable Poly(lactic acid) (PLA)/Poly(butylene adipate terephthalate) (PBAT) Blends. Polymers (Basel) 2023;15:881. https://doi.org/10.3390/POLYM15040881/S1.

[33] Andrzejewski J, Cheng J, Anstey A, Mohanty AK, Misra M. Development of Toughened Blends of Poly(lactic acid) and Poly(butylene adipate- co-terephthalate) for 3D Printing Applications: Compatibilization Methods and Material Performance Evaluation. ACS Sustain Chem Eng 2020;8:6576–89. https://doi.org/10.1021/ACSSUSCHEMENG.9B04925/SUPPL_FILE/SC9B04925_SI_001.PDF.

[34] Cardoso PHM, Coutinho RRTP, Drummond FR, da Conceição M do N, Thiré RM da SM. Evaluation of Printing Parameters on Porosity and Mechanical Properties of 3D Printed PLA/PBAT Blend Parts. Macromol Symp 2020;394. https://doi.org/10.1002/masy.202000157.

[35] Chen W, Qi C, Li Y, Tao H. The degradation investigation of biodegradable PLA/PBAT blend: Thermal stability, mechanical properties and PALS analysis. Radiat Phys Chem 2021;180. https://doi.org/10.1016/j.radphyschem.2020.109239.

[36] Appukuttan S, Joseph K. Immobilizing polymer chains in chlorobutyl rubber nanocomposites. Soc Plast Eng Plast Res Online 2014:1–2.

[37] Suhr J, Koratkar NA. Energy dissipation in carbon nanotube composites: A review. J Mater Sci 2008;43:4370–82. https://doi.org/10.1007/S10853-007-2440-X/METRICS.

[38] Razavi M, Wang SQ. Why Is Crystalline Poly(lactic acid) Brittle at Room Temperature? Macromolecules 2019;52:5429–41. https://doi.org/10.1021/ACS.MACROMOL.9B00595/SUPPL_FILE/MA9B00595_SI_005.MP4.

[39] Jian J, Xiangbin Z, Xianbo H. An overview on synthesis, properties and applications of poly(butylene-adipate-co-terephthalate)–PBAT. Adv Ind Eng Polym Res 2020;3:19–26. https://doi.org/10.1016/J.AIEPR.2020.01.001.

[40] Priya L, Jog JP. Poly(vinylidene fluoride)/clay nanocomposites prepared by melt intercalation: Crystallization and dynamic mechanical behavior studies. J Polym Sci Part B Polym Phys 2002;40:1682–9. https://doi.org/10.1002/POLB.10223.

[41] Aharoni SM. Increased glass transition temperature in motionally constrained semicrystalline polymers. Polym Adv Technol 1998;9:169–201.

[42] Liu T, Chen K. Influence of LLDPE on the mechanical properties improvement of 3D printed POE/LLDPE blends. J Vinyl Addit Technol 2024. https://doi.org/10.1002/VNL.22099.

[43] Qahtani M, Wu F, Misra M, Gregori S, Mielewski DF, Mohanty AK. Experimental Design of Sustainable 3D-Printed Poly(Lactic Acid)/Biobased Poly(Butylene Succinate) Blends via Fused Deposition Modeling. ACS Sustain Chem Eng 2019;7:14460–70. https://doi.org/10.1021/acssuschemeng.9b01830.

[44] Bellehumeur C, Li L, Sun Q, Gu P. Modeling of bond formation between polymer filaments in the fused deposition modeling process. J Manuf Process 2004;6:170–8. https://doi.org/10.1016/S1526-

6125(04)70071-7.

[45] Su S, Duhme M, Kopitzky R. Uncompatibilized pbat/pla blends: Manufacturability, miscibility and properties. Materials (Basel) 2020;13:1–17. https://doi.org/10.3390/ma13214897.

[46] Yeh J, Tsou C, Huang C, Chen K, Wu C, Chai W. Compatible and crystallization properties of poly(lactic acid)/poly(butylene adipate- co -terephthalate) blends. J Appl Polym Sci 2010;116:680–7. https://doi.org/10.1002/app.30907.

[47] da Costa FAT, Parra DF, Cardoso ECL, Güven O. PLA, PBAT, Cellulose Nanocrystals (CNCs), and Their Blends: Biodegradation, Compatibilization, and Nanoparticle Interactions. J Polym Environ 2023;31:4662–90. https://doi.org/10.1007/s10924-023-02899-7.

[48] Deng Y, Yu C, Wongwiwattana P, Thomas NL. Optimising Ductility of Poly(Lactic Acid)/Poly(Butylene Adipate-co-Terephthalate) Blends Through Co-continuous Phase Morphology. J Polym Environ 2018;26:3802–16. https://doi.org/10.1007/s10924-018-1256-x.

[49] Wei K, Zhu G, Tang Y, Tian G, Xie J. Thermomechanical properties of shape-memory hydro-epoxy resin. Smart Mater Struct 2012;21:55022.

[50] Leng J, Wu X, Liu Y. Effect of a linear monomer on the thermomechanical properties of epoxy shape-memory polymer. Smart Mater Struct 2009;18:95031.

[51] Rahmatabadi D, Aberoumand M, Soltanmohammadi K, Soleyman E, Ghasemi I, Baniassadi M, et al. 4D Printing-Encapsulated Polycaprolactone–Thermoplastic Polyurethane with High Shape Memory Performances. Adv Eng Mater 2023;25:2201309. https://doi.org/10.1002/adem.202201309.

Graphical Abstract

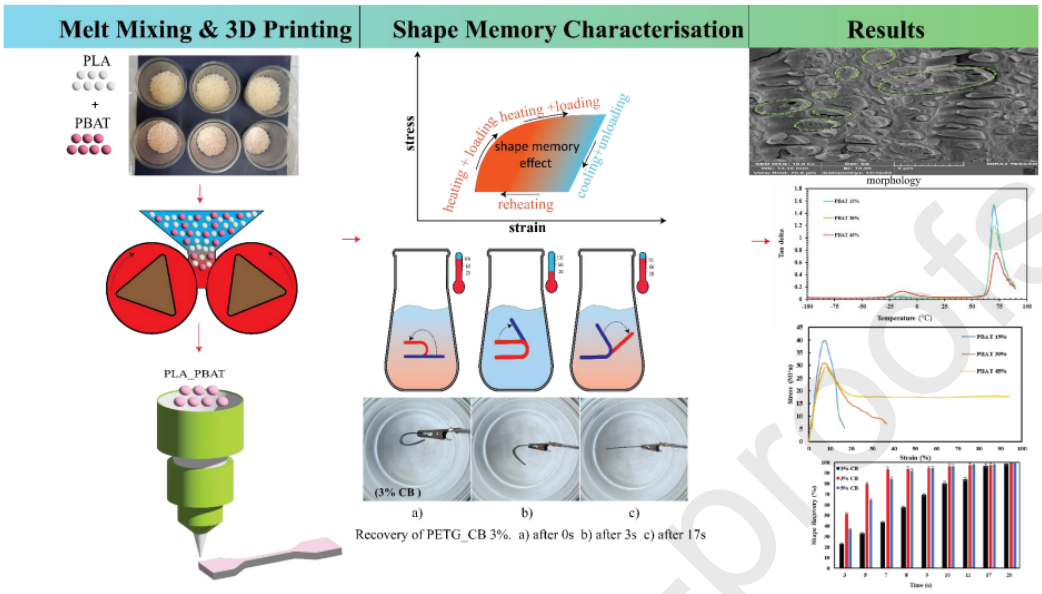

- **Conceptualization:** Davood Rahmatabadi.
- **Data curation:** Davood Rahmatabadi, Mahdi Khajepour, Abbas Bayati, and Kiandokht Mirasadi.
- **Formal analysis,** Davood Rahmatabadi and Mahdi Bodaghi
- **Writing—original draft:** Davood Rahmatabadi, Mahdi Khajepour, and Mahdi Bodaghi.
- **Investigation, Methodology, Writing—review & editing:** Davood Rahmatabadi, Mahdi Khajepour, Abbas Bayati, Kiandokht Mirasadi, Mohammad Amin Yousefi, Atefeh Shegeft, Ismaeil Ghasemi, Majid Baniassadi, Karen Abrinia, Mahdi Bodaghi, and Mostafa Baghani.
- **Supervision,** Ismaeil Ghasemi, Majid Baniassadi, Karen Abrinia, Mahdi Bodaghi, and Mostafa Baghani.

All authors have read and agreed to the final version of the manuscript.

☒ The authors declare that they have no known competing financial interests or personal relationships that could have appeared to influence the work reported in this paper.